ENVIRONMENTAL RESEARCH
LETTERS

LETTER • OPEN ACCESS

High spatial resolution ozone risk-assessment for Asian forests

To cite this article: Alessandra De Marco *et al* 2020 *Environ. Res. Lett.* **15** 104095

Environmental Research Letters

LETTER

High spatial resolution ozone risk-assessment for Asian forests

Alessandra De Marco[1,2], **Alessandro Anav**[1], **Pierre Sicard**[3], **Zhaozhong Feng**[4] **and Elena Paoletti**[2]

[1] Italian National Agency for New Technologies, Energy and the Environment (ENEA), Via Anguillarese 301, Rome, Italy
[2] IRET-CNR, Via Madonna del Piano, Sesto Fiorentino, Italy
[3] ARGANS, 260 route du Pin Montard, Biot 06410, France
[4] Institute of Ecology, Key Laboratory of Agrometeorology of Jiangsu Province, School of Applied Meteorology, Nanjing University of Information Science & Technology, Nanjing 210044, People's Republic of China

E-mail: alessandra.demarco@enea.it

Keywords: tropospheric ozone, phytotoxic ozone dose, forests, ozone risk-assessment, Asian forests

Supplementary material for this article is available online

OPEN ACCESS

RECEIVED
15 May 2020

REVISED
17 August 2020

ACCEPTED FOR PUBLICATION
3 September 2020

PUBLISHED
14 October 2020

Abstract

Background tropospheric ozone (O3) is increasing particularly over China and India, and becomes a major threat to Asian forests. By using the coupled WRF-Chem model at high spatial resolution (8 km) over Asia in 2015, we showed that both standards AOT40 (European) and W126 (United States) underestimated the O3 risk to deciduous forests and overestimated it to evergreen forests compared to the biologically based metric POD1. Both metrics AOT40 and W126 showed different spatial distribution and exceedance extent with respect to POD1. We found very high potential of O3 impacts on deciduous forest growth in Asia, while potential O3 impacts on evergreen forest types were lower. The most limiting factors were light availability, soil water content and air temperature (65%, 29% and 6%, respectively), making this region of the globe at high O3 risk for deciduous species and at medium O3 risk for evergreen species. For the first time, the O3 risk to Asian forests was quantified at high spatial resolution; and our results suggested: (i) a relevant overestimation of O3 risk to evergreen forests when using AOT40 and W126 relative to the more biologically based POD1 metric; and (ii) a significant underestimation of O3 risk to the boreal deciduous forests when using AOT40 and W126 relative to POD1 because of stomatal aperture permissive condition.

1. Introduction

Tropospheric ozone (O_3) is a seriously damaging air pollutant affecting human health (World Health Organisation 2013, Fu and Tai 2015, Cohen *et al* 2017), materials (Screpanti and De Marco 2009) and vegetation (Lu *et al* 2018, Mills *et al* 2018). Despite effective control efforts and legislation to reduce O_3 precursors emissions, such as nitrogen oxides (NO_x) and non-methanic volatile organic compounds (NMVOCs), surface O_3 pollution is still a major air quality issue over large regions of the globe (Sicard *et al* 2017, Gaudel *et al* 2018), and it is expected to increase in the future because of increasing methane emissions (Sicard *et al* 2017) and climate change (Anav *et al*, 2019). The high O_3 concentrations found over China and India megacities pose a major threat to food production and other ecosystem services in Asia (Tai *et al* 2014, Feng *et al* 2019, Zeng *et al* 2019).

Several studies reported the decrease of surface O_3 mean concentrations in United States (Lefohn *et al* 2010, Cooper *et al* 2012, Lin *et al* 2017) and Western Europe (Sicard *et al* 2013, Paoletti *et al* 2014, EEA 2016, Yan *et al* 2019). In contrast, in the last decades Asia became the world's largest emitter of O_3 precursors (Hoesly *et al* 2018). In particular, China emits 30% and 19% of the global emissions of NO_x and NMVOCs, respectively, followed by India with 13% and 11% (Hoesly *et al* 2018). Some region of East Asia have experienced decreases of O_3 precursors emission in recent years such as Beijing, the Pearl River Delta, Taiwan and Japan, and additional work is required to understand the response of surface O_3 (Duncan *et al* 2016, Krotkov *et al* 2016, Liu and Wang 2020). Recent analyses of Chinese O_3 monitoring stations (for the years 2015 and 2016) showed that O_3 levels were well above the threshold set to protect forests (Lu *et al* 2018, Feng *et al* 2019). All these considerations suggest that O_3 impacts on

vegetation is a relevant issue in Asia and thus warrant more investigations (Oksanen *et al* 2013, Feng *et al* 2015).

Due to the lack of observations with sufficient spatial and temporal coverage, especially in South Asia, many studies have used global and regional scale models to supplement the missing information from *in situ* measurements (Kunhikrishnan *et al* 2006, Engardt 2008, Sheel *et al* 2010). In the past decades, the important role of numerical models has been increasingly recognized and numerous air dispersion or air quality models were developed at various scales to assist in understanding, predicting and controlling air pollution (Lamarque *et al* 2013, Miranda *et al* 2015). These models were successfully applied to air pollution investigation and management in populated cities and regions worldwide (e.g. Reis *et al* 2005, Calori *et al* 2006, Haase *et al* 2014, Anav *et al* 2016).

The current O_3 pollution levels may lead to adverse effects on forest trees in East and Southeast Asia (Lu *et al* 2018) where high species richness is present (Kier *et al* 2009). Although some information on the O_3 effects on plants species in East Asia is available, the pollution situation of most Asian countries is not yet well clarified (Koike *et al* 2013). Main reason is the need of high-resolution regional model, to provide better estimates of air pollution with a lower bias and the second one is the low availability of tropospheric air quality measurements, needed for model validation. Indeed mostly of the modelling information available for Asia are from global models at horizontal resolution of e.g. ~50 km (Engardt 2008). Several air quality or chemical transport models (CTMs) have been developed and ran to represent the complex mechanisms involved in transport, transformation and deposition processes in East Asia (Han 2007). The CTMs were applied to study air pollution for China as a whole (Hu *et al* 2016, Li *et al* 2016) and for several Chinese regions (Wang *et al* 2012, Liao *et al* 2015). Hu *et al* (2016) applied the Community Multi-scale Air Quality (CMAQ) and Weather Research Forecasting (WRF) modelling system to predict air pollutant concentrations over China. The results showed an overestimation of 1 h and 8 h O_3 averages, probably due to the coarse horizontal resolution (36 km). A modified WRF-CMAQ modelling system was used to simulate O_3 concentrations in winter (December 2014–February 2015) and summer (June–August 2015) for the Sichuan Basin (Qiao *et al* 2019). Most of the basin was found to exceed the World Health Organisation (WHO) guidelines for 8 h O_3 on >70% of winter days and >40% of summer days. The 1 h and 8 h O_3 averages were both greatly over-predicted in winter, but the model performance was acceptable in summer, when the photochemical production of O_3 due to anthropogenic emissions should be strongest in the basin (Qiao *et al* 2019).

The availability of station data used to validation chemistry models was a main issue in this area due to the scarcity of monitored information (Li *et al* 2007). Recently, few authors have validated CTMs results with *in situ* and satellite observations (e.g. Kumar *et al* 2012, Sharma *et al* 2016, Sicard *et al* 2020). As an example, the WRF-CMAQ model was used in India with different spatial resolution for emissions and meteorological inputs (e.g. 36 km) to assess source and species sensitivities of ground-level O_3 concentrations (Chatani *et al* 2014, Sharma *et al* 2016). Simulations of O_3 and its precursors have been conducted using the updated version-2 (HTAP-v2) emission inventory and the offline global chemistry transport model MOZART-4 (Surendran *et al* 2015), showing reasonable model performance, but some disagreement in O_3 concentrations and seasonal variation over South Asia were still evident (Surendran *et al* 2015).

Forests in Asia are important for carbon sequestration (Fang *et al* 2001, Yu *et al* 2014) and biodiversity conservation (Myers *et al* 2000). China has been implementing the most ambitious afforestation programs in the world (Zhang *et al* 2017). Thus, it is important to estimate O_3 impacts on forest ecosystems in an area characterized by many different climatic conditions and plant species (Xu *et al* 2010).

Different criteria have been developed to define O_3 risk assessment for forests (Lefohn *et al* 2018). A concentration-based metric, i.e. AOT40 defined as the sum of hourly O_3 concentration exceeding 40 ppb across daily and seasonal time windows, is currently used in the European legislation for O_3 risk assessment (CLRTAP 2017). The second metric, i.e. PODY, developed more recently in Europe, is based on phytotoxic O_3 dose entering the leaves, depending on the stomatal aperture (Paoletti and Manning 2007), with an hourly threshold Y that is set to 1 nmol m^{-2} s^{-1} for forests (CLRTAP 2017). The two metrics showed inconsistent spatial (Anav *et al* 2016) and temporal patterns (De Marco *et al* 2015) from local to regional scales over Europe. The current standard recommended in United States for forest protection is W126 (US Federal Register 2015), defined as the sum of the hourly O_3 concentrations during the growing season, and each concentration is weighted by a sigmoidal function to assign greater emphasis to the highest concentrations (Lefohn *et al* 2018). Ozone critical levels (CLs) were developed for the three metrics, intended as dose (POD1) or concentration below which no effect on forests is expected (Büker *et al* 2015), that showed a different sensitivity between evergreen (lower) and deciduous species (higher) (Sicard *et al* 2016). Information on PODY in Asia is still limited to specific countries by modelling approaches (e.g. Japan, Hoshika *et al* 2017) or specific locations with poplar only (Hu *et al* 2015, Shang *et al* 2017). Tang *et al* (2013) evaluated the magnitude and distribution of O_3-induced

wheat production loss in China and India using flux-based methods (POD6) and compared different O_3 dose metrics (AOT40 and POD6) with a resolution of 40 km. At the moment, similar risk assessment is not available for forests in the same region. Therefore, there is an urgent need to perform regional simulations of POD1 to provide high spatial resolution inputs for a more realistic O_3 risk assessment for forests over Asia.

The main aims of the present study were to (i) evaluate magnitude and distribution of O3 risk to Asian forests at high spatial resolution, by comparing concentration-based (AOT40 and W126) and uptake-based (POD1) metrics; (ii) assess the spatial consistency between metrics in order to identify areas where they disagree; (iii) quantify the percentage of the Asian domain exposed to O3 levels exceeding the thresholds of protection for evergreen and deciduous forests in northern, continental and (sub)tropical climates; and (iv) identify the most important climate constraints affecting the stomatal uptake of O3 by Asian forests. We hypothesized that AOT40, W126 and POD1 are uncoupled, and that deciduous forests are at higher risk than evergreen forests, as suggested by a meta-analysis of experimental results in Asia (Li *et al* 2017).

2. Methods

2.1. WRF-Chem model

We used the Weather Research and Forecasting model (WRF-Chem, v3.9), a coupled climate-chemistry model (Grell *et al* 2005, Skamarock and Klemp 2008), to reproduce the regional climate and surface O_3 concentrations over South-Eastern Asia. The model domain (figure 1) is projected on a lambert conformal map with a horizontal resolution of 8 km, which allows to simulate atmospheric chemical and physical processes at fine spatial scale. The entire year 2015 was simulated, with a spin up of 1 month (1st–31st December 2014).

The initial and boundary conditions for meteorology, updated every 3 h, were retrieved from the European Centre for Medium-range Weather Forecast ERA5 product (C3S-ERA5 2017), whose outputs are available with a horizontal resolution of ~31 km. Similarly, chemical boundary conditions were provided from MOZART-4 (Model for OZone And Related chemical Tracers) every 6 h (Emmons *et al* 2010) with a horizontal resolution of ~180 × 240 km. We used the MOZART scheme to simulate atmospheric chemistry, the MEGAN (Model of Emissions of Gases and Aerosols from Nature) model to estimate biogenic emissions (Guenther *et al* 2012), while fire emissions were taken from the FINN (Fire INventory from NCAR, v1.5) inventory (Wiedinmyer *et al* 2011). Monthly varying anthropogenic emissions were based on the EDGAR-HTAP (Emission Database for Global Atmospheric Research for Hemispheric Transport of Air Pollution, v2.2) inventory (Janssens-Maenhout *et al* 2015) which is available on a grid of ~10 × 10 km for the year 2010. Ozone concentrations obtained by the model were considered as top of the forest canopy, because the first layer of WRF/Chem is around 30 m height. The model validation is not showed in this manuscript, but is fully reported by Sicard *et al* (2020).

2.2. Definition of the forest types

The dominant forest distribution (figure 1) was obtained by merging the USGS landcover distribution and the Koppen climate, following the methodology proposed by Anav *et al* (2016). This allows using the vegetation definition and the parameterizations described in chapter 3 of the Mapping Manual (CLRTAP 2017) and computing the POD1 and its CL derivation. The six categories of forests identified are boreal deciduous (BD), boreal evergreen (BE), continental deciduous (CD), continental evergreen (CE), (sub)tropical deciduous (TD), and (sub)tropical evergreen (TE) species. For boreal and continental types, we used the parameterization developed by CLRTAP (2017) for beech/birch (deciduous) and Norway spruce (evergreen). Due to the lack of specific tropical and sub-tropical forest parameterization in CLRTAP (2017) and in the scientific literature, we decided to join tropical and sub-tropical forest species in a single category and approximate the (sub)tropical species to Mediterranean species. Indeed, the Koppen classification includes both sub-tropical and Mediterranean climates into the same category C of temperate climates (Kottek *et al* 2006). For the (sub)tropical type, we thus selected the parameterization suggested for Mediterranean conditions (CLRTAP 2017) for deciduous oaks (TD) and evergreen oak (TE).

2.3. Estimation of AOT40, W126 and POD1 metrics

AOT40 (expressed in ppm h) was computed according to the following formulation (CLRTAP 2017), i.e. as the sum of the hourly exceedances above 40 ppb over the time window between start date of the growing season (SGS) and end date of the growing season (EGS) according to figure 2, during daylight hours:

$$\mathrm{AOT40} = \int_{SGS}^{EGS} \max\left([O_3] - 40{,}0\right) \mathrm{d}t \qquad (1)$$

where $[O_3]$ is the hourly O_3 concentration (ppb) and dt is the time step (1 h). The function 'maximum' ensures that only values exceeding 40 ppb are included.

The W126 exposure index (expressed as ppm h) is a non-threshold index that is described as the sigmoidal weighting sum of hourly O_3 concentrations recorded during specified daily and seasonal time windows, where each hourly O_3 value is

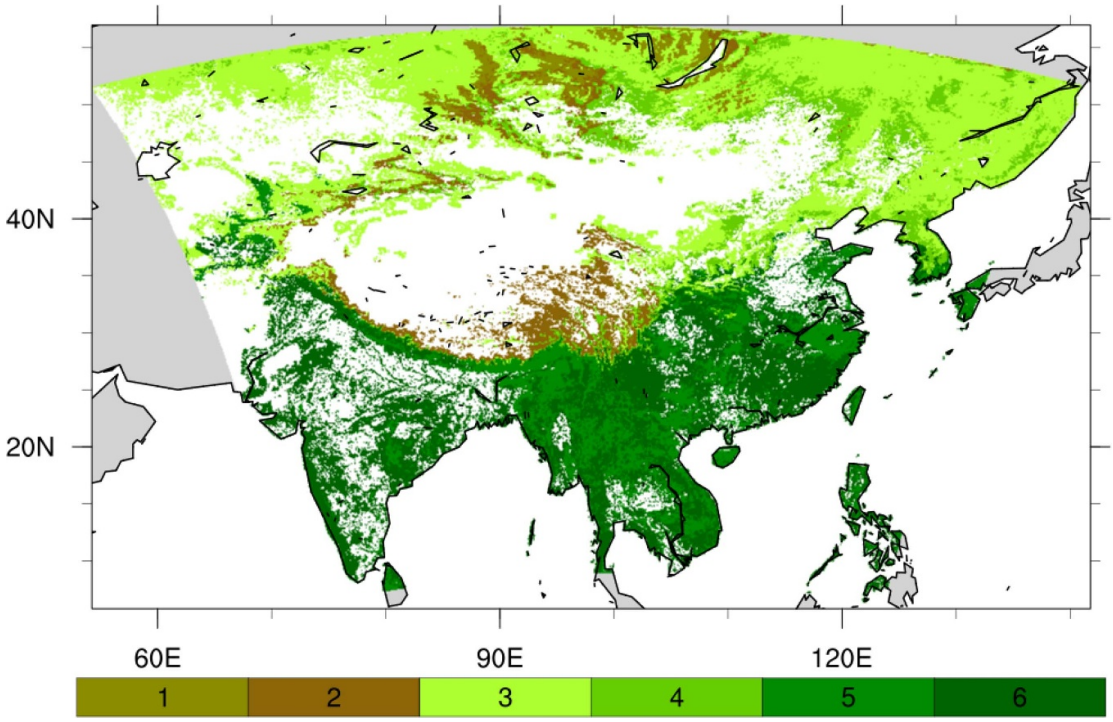

Figure 1. Classification of forest types of Asia, according to the parameterization in CLRTAP (2017). 1 = Boreal Deciduous (BD); 2 = Boreal Evergreen (BE); 3 = Continental Deciduous (CD); 4 = Continental Evergreen (CE); 5 = (Sub)tropical Deciduous (TD); 6 = (Sub)tropical Evergreen (TE). Details on the parameterization are in the text. White color represents grid points without forest cover, and grey color is used outside the domain.

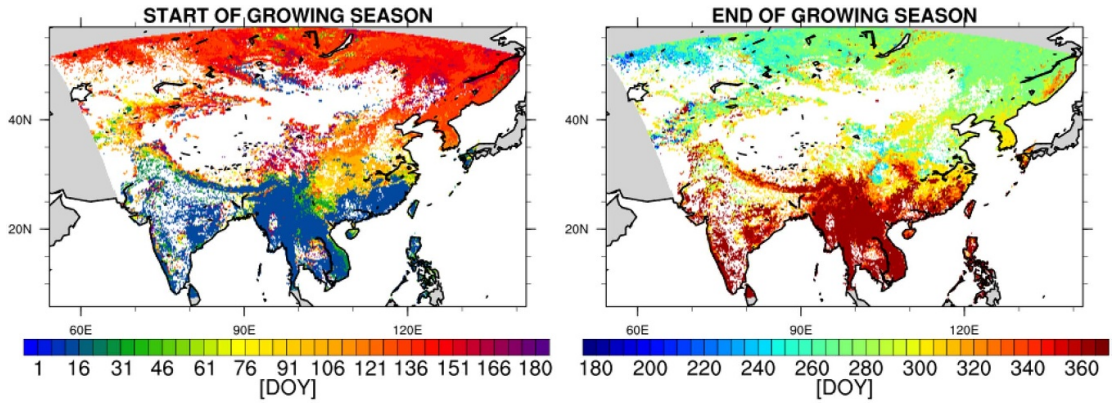

Figure 2. Day of the year (DOY) for start of the growing season and end of the growing season over Asian forests. White color represents grid points without forest cover, and grey color is used outside the domain.

given a weight that increases from zero to one with increasing value (Lefohn *et al* 2018) and is defined as follows:

$$\mathrm{W126} = \Sigma\, W_i \times C_i \tag{2}$$

$$W_i = \frac{1}{\left[1 + M \times exp\ \left(-A \times \frac{C_i}{1000}\right)\right]} \tag{3}$$

where $M = 4403$, $A = 126$, and C_i is the hourly average O_3 mixing ratio in ppb. Further details about the index are available in Lefohn *et al* (2018). For consistency W126 and ATO40 were cumulated during the same daylight hours and growing season.

For the PODY, we applied a threshold Y of 1 nmol m^{-2} s^{-1} for consistency with the approach recommended by CLRTAP (2017) for forest protection; the POD1 was computed as follows (Simpson *et al* 2007, Tuovinen *et al* 2007, Büker *et al* 2015, CLRTAP 2017):

$$\mathrm{POD1} = \int_{SGS}^{EGS} \max\left(\frac{R_c}{R_b + R_c} \times g_{sto} \times [\mathrm{O_3}] - 1, 0\right) \mathrm{d}t \tag{4}$$

where dt is 1 h, [O_3] is the hourly O_3 concentrations (ppb), R_b is the quasi-laminar resistance (s m^{-1}), R_c is the leaf surface resistance (s m^{-1}), and g_{sto} is the hourly value of stomatal conductance to O_3 (mmol O_3 m^{-2} PLA s^{-1}, where PLA is the Projected Leaf Area) computed as following.

$$g_{sto} = g_{\max} * f_{phen} * f_{light} * \max(f_{\min}, f_{temp} * f_{VPD} * f_{SWC}) \quad (5)$$

where g_{sto} is the actual stomatal conductance and g_{max} is the maximum stomatal conductance of a plant species (mmol O_3 m^{-2} PLA s^{-1}) expressed on a projected total leaf surface area. The functions f_{light}, f_{temp}, f_{VPD}, and are the variation in the maximum species-specific stomatal conductance g_{max} with photosynthetically flux density at the leaf surface (PPFD μmol photons m^{-2} s^{-1}), surface air temperature (T, °C), vapor pressure deficit (VPD, kPa), and volumetric soil water content (SWC, m^3 m^{-3}), respectively. The function $f_{\min}$ is the minimum stomatal conductance. These species-specific functions vary between 0 and 1, with 1 meaning no limitation to g_{sto}, and are expressed as CLRTAP (2017):

$$f_{light} = 1 - e^{(-light_a \times PPFD)} \quad (6)$$

$$f_{temp} = \left(\frac{T - T_{\min}}{T_{\text{opt}} - T_{\min}}\right) * \left[\left(\frac{T_{\max} - T}{T_{\max} - T_{\text{opt}}}\right)^{\left(\frac{T_{\max} - T_{\text{opt}}}{T_{\text{opt}} - T_{\min}}\right)}\right] \quad (7)$$

$$f_{VPD} = \min\left\{1, \max\left[f_{\min}, \times \left(\frac{(1 - f_{\min}) * (VPD_{\min} - VPD)}{VPD_{\min} - VPD_{\max}}\right) + f_{\min}\right]\right\} \quad (8)$$

$$f_{SWC} = \min\left[1, \max\left(f_{\min}, \frac{SWC - WP}{FC - WP}\right)\right] \quad (9)$$

where $light_a$ is a dimensionless constant, PPFD is hourly photosynthetic photon flux density, T_{opt}, $T_{\min}$, and $T_{\max}$ represent the optimum, minimum, and maximum temperature for g_{sto}, $VPD_{\min}$ and $VPD_{\max}$ are minimum and maximum VPD for g_{sto}, and WP and FC are the soil water content at wilting point and field capacity, respectively (Anav *et al* 2016, CLRTAP 2017).

In addition, $f_{\min}$ is the species-specific fraction of $g_{\max}$ and f_{phen}, i.e. the phenology of vegetation, is used to compute the duration of the growing season during which plants can uptake O_3. In detail, we used the seasonal variation of third generation Leaf Area Index, i.e. bi-weekly LAI3g data with ~8 km of spatial resolution (Zhu *et al* 2013) to define the start of the growing season (SGS) and end of the growing season (EGS) (figure 2), as described by Anav *et al* (2018).

2.4. Calculation of CL exceedances and biomass losses

CLs are defined as '*concentrations, cumulative exposure or cumulative stomatal flux of atmospheric pollutants above which direct adverse effects on sensitive vegetation may occur according to present knowledge*' (CLRTAP 2017). The parameter usually evaluated for estimating such adverse effect on forests is a 4% reduction in biomass except for evergreen species where the biomass reduction is set to 2% (CLRTAP 2017). Exceedances of O_3 CL were calculated for the three metrics AOT40, W126 and POD1 as recommended by CLRTAP (2017), i.e. as difference between the estimated value in each grid cell and the CL obtained by literature data. We used different CLs depending on the metric, i.e.: for AOT40 we applied the European CL set to 5 ppm h to protect all forests types (CLRTAP 2015); for W126, we used 7 ppm h or 21 ppm h, as recommended by Environmental Protection Agency (EPA 2007) to protect the most sensitive tree species or any kind of vegetation; for POD1, we used 5.2 mmol m^{-2} for BD and CD, 9.2 mmol m^{-2} for BE and CE, 14.0 mmol m^{-2} for TD and 47.3 mmol m^{-2} for TE, according to CLRTAP (2017).

After performing a point-wise calculation of the exceedances over the model domain, the non-attainment area of the target value (in %) was calculated relative to the total domain covered by either deciduous or evergreen forests. The biomass losses for each forest type were estimated based on the dose-response functions derived by CLRTAP (2017), as indicated in table S1 (available online at https://stacks.iop.org/ERL/15/104095/mmedia).

3. Results

The lowest AOT40 levels were found in South Asia (i.e. Vietnam, Laos and Thailand) dominated by moist and dry broadleaf forest types (figure 1) and with lower O_3 concentrations (figure 3). The area with highest AOT40 values was observed in central China, characterized by high O_3 concentrations, especially during growing season (Sicard *et al* 2020) and in the Indo-Gangetic Plain region, characterized mainly by high-elevation forests e.g. Himalaya (figure 1). The spatial distribution of W126 was similar to AOT40, but the highest and lowest values were amplified due to the nature of the metric. Peaks of W126 were located mainly in Northern and Northeastern India (figure 3).

In contrast, the spatial pattern of POD1 was different from that of AOT40 and W126 (figure 3), with the highest absorbed dose for TD and TE forests and the lowest for BE forests (figure 4). A different spatial distribution of hot-spots was observed in the southern region, with the highest POD1 values in southern China rather than in India (figure 3). The average spatial correlation coefficient was 0.96 between AOT40

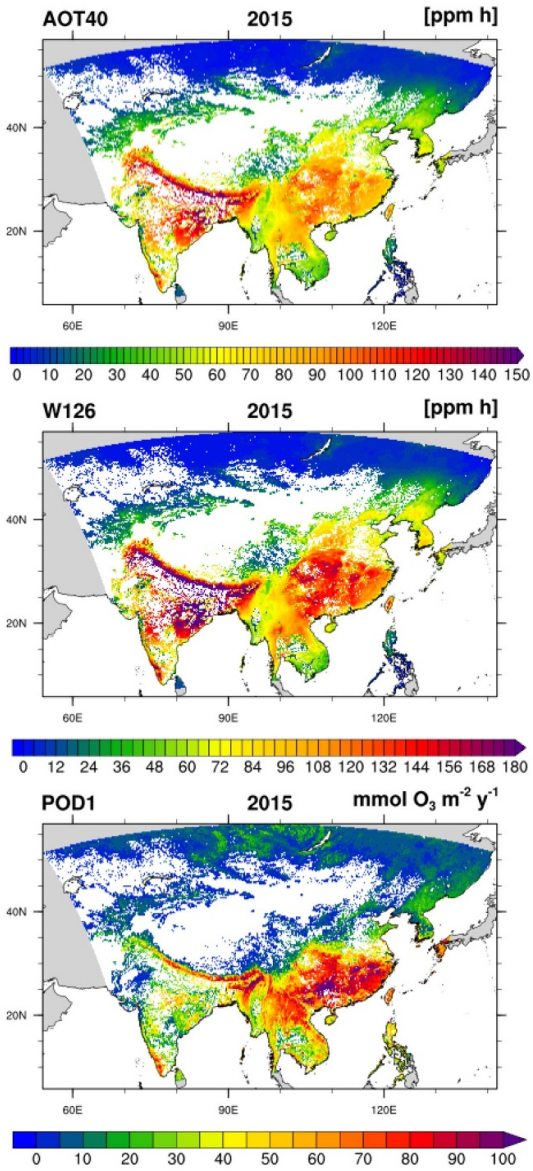

Figure 3. Ozone risk assessment for Asian forests estimated by three metrics (AOT40, W126 and POD1) in 2015. White color represents grid points without forest cover and grey color is used outside the domain.

and W126 and 0.20 between AOT40 and POD1 (data not shown).

The selected metrics split in terms of dominant vegetation are displayed in figure 4; our results indicate that, in 2015 the lowest AOT40 and W126 values were found in the northern region (figure 3) dominated by boreal or continental forest species (figure 1), while the highest AOT40 and W126 values were observed in the areas where tropical and subtropical forests grow (figure 4).

Considering the CLs, our results indicate that the AOT40 CL was exceeded over 53%, 93%, 74%, 86%, 98% and 97% of the areas covered by BD, BE, CD, CE, TD and TE forest types, respectively (figure 5). The W126 CL recommended for protecting sensitive plant species was exceeded over 31%, 87%, 57%, 73%, 98% and 98% of the areas covered by BD, BE, CD, CE, TD and TE forest types, respectively, while the exceedances of the W126 CL for the protection of all species covered 5%, 59%, 28%, 43%, 93% and 94% of the areas covered by BD, BE, CD, CE, TD and TE forest types, respectively. For both AOT40 and W126, the main attainment areas (i.e. achieving the air-quality standard) were in boreal and continental climates, with deciduous species showing lower risk than evergreen species. Regarding the POD1, 99%, 12%, 65%, 18%, 93% and 46% of the areas covered by BD, BE, CD, CE, TD and TE forest types exceeded the respective CLs (figure 5). The POD1-based O_3 risk was higher for deciduous forests than evergreen forests, despite the shorter duration of the growing season.

To link the POD1 to the forests biomass loss, we applied the dose-response function to the different forests type. The average POD1-driven biomass loss for the six forest types is shown in figure 6. The

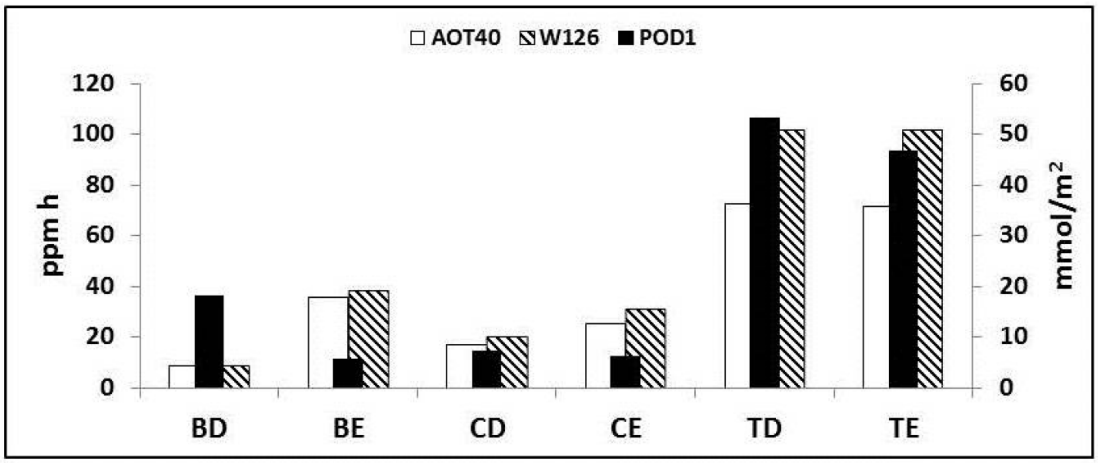

Figure 4. Average value of AOT40 (white bars), W126 (line bars) and POD1 (black bars) in the six forest types: B, Boreal; C, Continental; T, (sub)tropical; D, deciduous; E, evergreen.

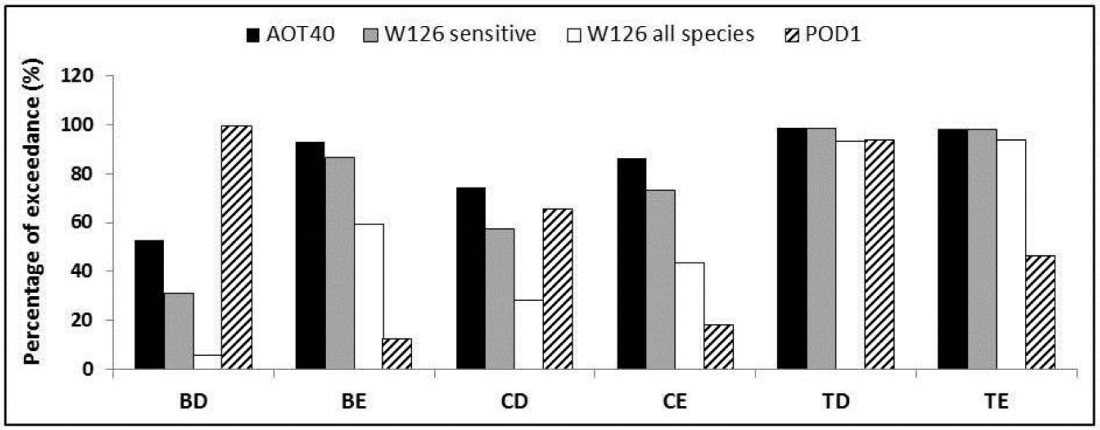

Figure 5. Non-attainment area (in %) for Asian forests exposed to ozone levels exceeding the critical levels for each metric in 2015. Forest types: B, Boreal; C, Continental; T, (sub)tropical; D, deciduous; E, evergreen.

most POD1-affected forest types were the deciduous species, in particular BD and TD, with a respective biomass loss of 16% and 17%. The CD showed a biomass reduction of 7%, while evergreen species showed lower biomass reductions, even if the accumulation period was longer. Indeed, a biomass loss of 1.5%, 1.6% and 4.4% was estimated for BE, CE and TE species, respectively. When all forests were averaged, the POD1-estimated biomass loss was 7%.

The spatial distribution of the limiting functions *f*, i.e. the functions regulating the stomatal opening and consequently the O3 uptake by leaves, is shown in figure 7.

Considering the temperature, we found a relevant limitation to stomatal opening only in the mountainous region around the Tibetan plateau, while in the remaining area of the domain the air temperature is not significantly limiting O3 uptake. In contrast, the maximum f_{light} limitation was observed in the south-eastern area of the domain, and this function was relatively low (i.e. high limitation) over the whole domain. f_{VPD} was generally not limiting for stomatal conductance in Asia, except in the central-western part of the domain, while f_{SWC} was strongly limiting for stomatal conductance over almost all India and the central part of the domain. The average values of the 4 limitation functions in the six forest types is shown in figure 8. As expected f_{temp} is mostly limiting for stomatal conductance in boreal forests (0.62 and 0.44 for BD and BE, respectively), and f_{light} is mostly limiting stomatal conductance in tropical forests (0.46 and 0.48 for TD and TE, respectively), while intermediate values were found in the continental forests for both CD and CE, where f_{SWC} limitation seems to be more relevant (0.56 and 0.51 for CD and CE, respectively)

By selecting the most limiting function in each cell grid, we observed that the most distributed limiting function over Asia was f_{light} (over 65% of the domain), followed by f_{SWC} (29%) and f_{temp} (6%) (figure 9). Just in few grid points (<1%) the most limiting function was f_{VPD}.

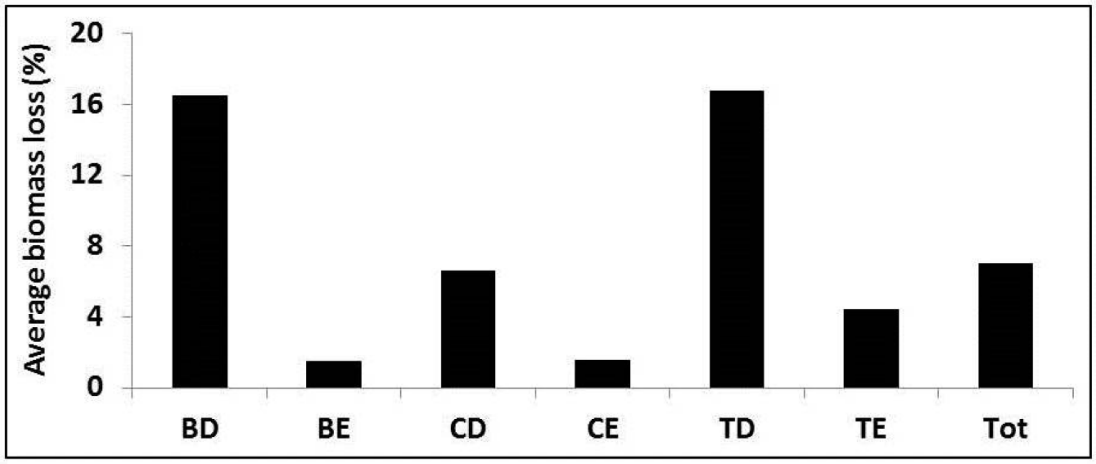

Figure 6. Average biomass loss due to cumulative stomatal ozone uptake (POD1) for the six forest types over the Asian domain, expressed as an average on all forests (Tot) or per forest type. Forest types: B, Boreal; C, Continental; T, (sub)tropical; D, deciduous; E, evergreen.

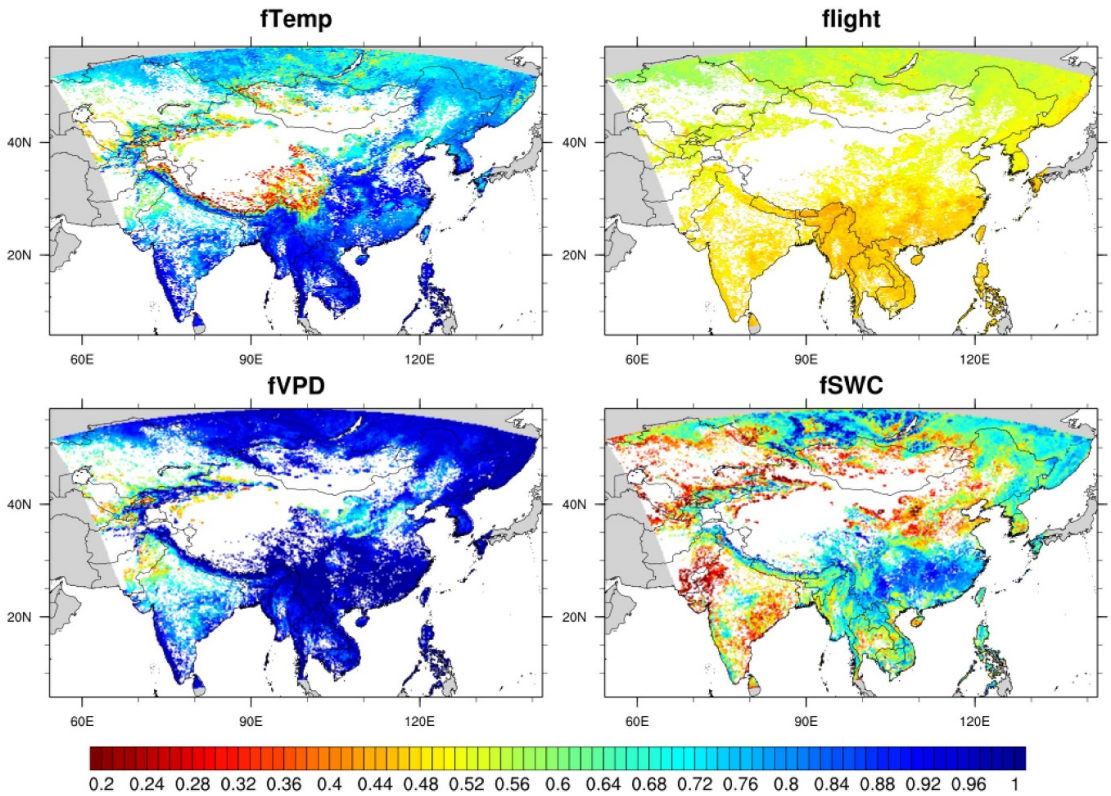

Figure 7. Average limitation of stomatal conductance due to temperature (f_{temp}), solar radiation (f_{light}), vapor pressure deficit (f_{VPD}) and soil water content (f_{SWC}) over Asian forests in the year 2015. The values are dimensionless, ranging from 0 (maximum limitation) to 1 (no limitation). Withe color represents grid points without forest cover, and grey color is used outside the domain.

4. Discussion

East and South Asia has recently experienced rapid economic growth, during which anthropogenic emissions have increased and deteriorated air quality (Kurokawa and Ohara 2019). Air pollution, especially surface O_3 in East and Southeast Asia, is more serious than in Europe and North America (Koike *et al* 2013, Mills *et al* 2018) and is still expected to increase by 2100 (Sicard *et al* 2017). Thus, the use of air quality models has also increased in this region to better understand the spatial and temporal distributions of air pollutants and to examine the impact of the increased anthropogenic emissions on air quality degradation for Asian countries (Park and Kim 2014) and consequently the impacts on forests (Feng *et al* 2019).

In this study, we used WRF-Chem with a high horizontal resolution (8 km) over a domain covering all India, China, part of southern Asia, and

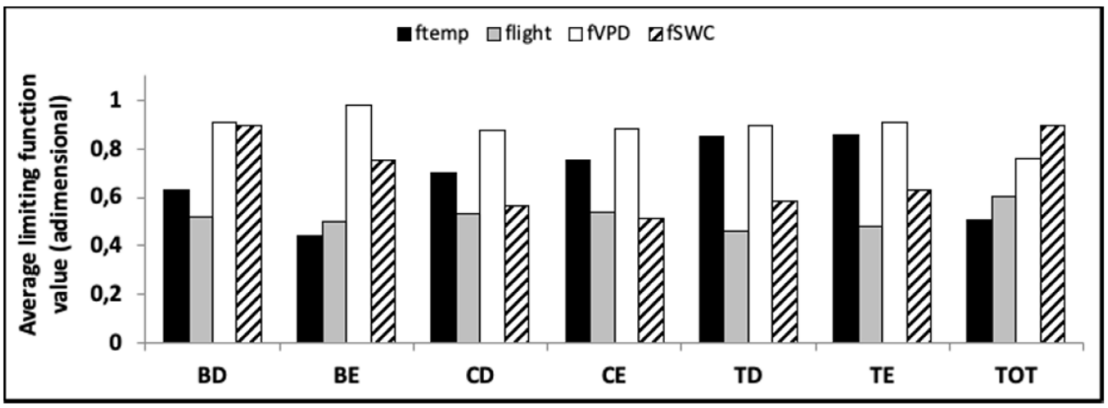

Figure 8. Average limitation function values for the six forest types over the Asian domain, expressed as an average on all forests (TOT) or per forest type. Forest types: B, Boreal; C, Continental; T, (sub)tropical; D, deciduous; E, evergreen. Black bars indicated f_{temp}, grey bars f_{light}, white bars f_{VPD} and striped bars indicated f_{SWC}.

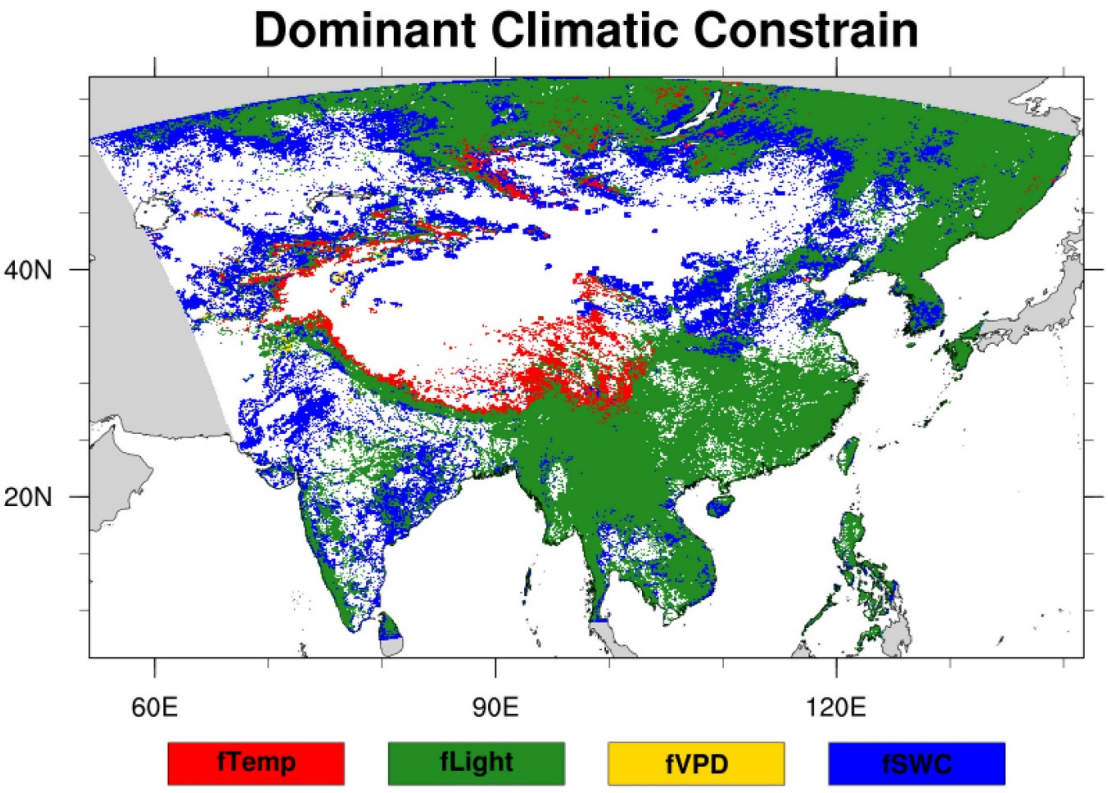

Figure 9. Distribution of the most limiting function per each grid cell (temperature in red, light in green, vapor pressure deficit (*VPD*) in yellow and soil water content (*SWC*) in blue) over the Asian forests in 2015. White color represents grid points without forest cover, and grey color is used outside the domain.

reaching southern Siberia. The same model was previously used to simulate ground-level O_3 over a smaller domain in East Asia (Park *et al* 2014), and emphasized the importance of the resolution in the performance of the model. For this reason, we selected a fine spatial resolution to have more realistic results. Our simulation was validated against *in-situ* measurements from monitoring stations across China and satellite data (Sicard *et al* 2020); the comparison with measurements suggests that the model well reproduces the spatial pattern of meteorological variables and surface O_3 concentration. Indeed, the WRF-Chem model simulated well the spatial distribution and seasonal variation of O_3. Compared to IASI-GOME2 satellite retrievals, a good spatial agreement is noticed in summer, with a spatial correlation of 0.99, and a lower correlation is observed during spring and winter (0.61 and 0.71, respectively). Compared to ground observations data (from 1500 air quality monitoring network across China), a mean annual bias of 5 ppb is observed in 2015. This bias is in line with the ones showed by

the European regional models described in Colette *et al* (2011). Looking at the surface air temperature, one of the most important parameter affecting POD1 entity, WRF captures well the spatial pattern with a decreasing south-north gradient and a cold area over the Tibetan plateau (Sicard *et al* 2020).

Interestingly, the POD1 values were consistent with the results shown for Europe (Anav *et al* 2016), while AOT40 values were around 100%–200% higher in Asia than in Europe. The latter result is consistent with Lu *et al* (2018), that found significantly higher AOT40 and W126 levels in China, i.e. 35%–100% and 50%–170% higher than in Europe and United States, respectively.

Asian studies implementing PODY are fewer for trees than for crop species (Agathokleous *et al* 2018), and have normally provided experimental observations in very local plots and for a few species. POD1 is the index recommended by CLRTAP (2017) for protecting trees against O_3-induced biomass loss. In an experiment with poplars in China, AOT40 and POD1 dose-response relationships indicated a 5% biomass loss at 12.0 ppm h and 6.1 mmol m^{-2}, respectively (Hu *et al* 2015). To calculate the exceedance, we used the thresholds, dose-responses and CLs set in Europe (CLRTAP 2017) because the only PODY-based dose-response relationships for Asia are for hybrid poplar and thus insufficient to represent the variety of forest types in Asia. Our results showed different sensitivity of forest types to O_3 concentrations potential exposure (AOT40 and W126) or O_3 fluxes (POD1), in particular with respect to the non-attainment area for forest protection. Most of evergreen forests (86%–97%) were potentially exposed to O_3 concentrations exceeding the limits for forest protection while the percentage of evergreen forests exposed to POD1 above the CLs was lower (12%–46%). Asian studies should focus on flux-based O_3 metrics to provide relevant bases for developing proper standards. However, given the technical requirements in calculating flux-based O_3 metrics, which can be an important limitation in developing countries, cumulative exposure indices like AOT40 should always accompany flux-based indices (Agathokleous *et al* 2018).

A different spatial distribution of AOT40 and POD1 in East Asia was previously described by Hoshika *et al* (2011) and by De Marco *et al* (2015) and Anav *et al* (2016) in Europe. In particular in Asia POD0 values ranging from 10 to 48 mmol m^{-2} were reported (Hoshika *et al* 2011), while in our results we obtained values of similar magnitude, but with an hourly threshold Y of 1 nmol m^{-2} s^{-1}. Our spatial variability was in line with the spatial distribution obtained by Hoshika *et al* (2011). We obtained similar results with no limitation due to *VPD* on the major part of the domain, excluding the central north-western part of India. One possible explanation is that the Tibetan Plateau (mean elevation over 4000 m a.s.l.) acting as a strong heat source in summer, generates upward airflow motions over its eastern flank that, combined with large amounts of moisture from the tropics, result in strong monsoons and wet climate in East Asia (Ding and Chan 2005).

The limiting functions are important to determine the role of climatic conditions on stomatal conductance (Emberson *et al* 2007). Physiological responses to changes in climate are highly dependent on the limiting factors of a particular site to forest growth. The eastern part of the domain did not show *SWC* as most limiting factor, while the western part of the domain, including India, with either limited rainfall or high temperature showed some areas characterized by limiting soil moisture, a very important function in many dry area of the globe (De Marco *et al* 2016). We showed that the most limiting function to O_3 uptake in eastern Asia was f_{light}, in agreement with Nemani *et al* (2003) that investigated geographic distribution of potential climatic constraints to plant growth derived from long-term climate statistics. As the exchange of gases between atmosphere and terrestrial vegetation is regulated by stomata opening, air pollutants may take advantage of the stomatal aperture to enter leaves, suggesting that the temporal evolution of O_3 and CO_2 uptake are consistent. Indeed Melillo *et al* (1993) found that the predicted NPP decreases for tropical evergreen forest, may be related to increased temperature and cloudiness. It is important to note that f_{light} estimation included nighttime hours, and thus is affected by the duration of daylight hours. Similar analysis was done in Europe (Emberson *et al* 2007, Anav *et al* 2019) to identify the key drivers determining O_3 flux by tree species and region. In Europe a key driver for PODY variation was the length of the growing season (f_{phen}), which increased and counteracted the negative trend in O_3 concentrations leading to a limited PODY increase during the time period 2000–2014 (Anav *et al* 2019). Epidemiological studies where PODY is compared with observed impact on vegetation would help in selecting the best metric to estimate the O_3 risk for forests in Asia (Sicard *et al* 2016, Braun *et al* 2017). Some evidences showed the higher performance of O_3 flux instead of exposure to estimate the impacts of O_3 on forest trees in Europe (De Marco *et al* 2015, Sicard *et al* 2016, Paoletti *et al* 2019).

5. Conclusions

The lack of information still presents in Asia in terms of stomatal O_3 uptake by the forests, both for modelling and *in-situ* measurements, warrant more intense studies in this region of the globe. To bridge this gap of knowledge we performed, for the first time, a risk assessment on Asian forests using a high spatial resolution model in order to estimate the phytotoxic O_3 uptake (POD1) into the tree leaves for six

forest types, highlighting its spatial distribution compare to concentration-based metrics. We found very high potential of O_3 impacts on deciduous forest growth in Asia, while potential O_3 impacts on evergreen forest types were lower. In particular, the limiting conditions of light, soil water content and temperature in a context of climate change, make this region of the globe at high O_3 risk for deciduous species and medium O_3 risk for evergreen species.

Acknowledgments

This work was carried out with the contribution of: LIFE financial instrument of the European Union (LIFE15 ENV/IT/000183) in the framework of the MOTTLES project '*Monitoring ozone injury for setting new critical levels*'; National Key Research and Development Program of China, Grant/Award Number: 2017YFC0210106; National Natural Science Foundation of China (No. 41771034); Chinese Academy of Sciences President's International Fellowship Initiative (PIFI) for Senior Scientists (2016VBA057); and CNR-CAS bilateral agreement 2017–2019 '*Ozone impacts on plant ecosystems in China and Italy*'.

Data availability statement

The data that support the findings of this study are available upon reasonable request from the authors.

ORCID iD

Alessandro Anav https://orcid.org/0000-0002-4217-7563

References

Agathokleous E, Kitao M and Kinose Y 2018 A review study on O_3 phytotoxicity metrics for setting critical levels in Asia *Asian J. Atmos. Environ.* **12** 1–16

Anav A *et al* 2019 Growing season extension affects ozone uptake by European forests *Sci. Total Environ.* **669** 1043–52

Anav A *et al* 2016 Comparing concentration-based (AOT40) and stomatal uptake (PODY) metrics for ozone risk assessment to European forests *Glob. Change Biol.* **22** 1608–27

Anav A, Liu Q, De Marco A, Proietti C, Savi F, Paoletti E and Piao S 2018 The role of plant phenology in stomatal ozone flux modelling *Glob. Change Biol.* **24** 235–48

Braun S, Achermann B, De Marco A, Pleijel H, Karlsson P E, Rihm B, Schindler C and Paoletti E 2017 Epidemiological analysis of ozone and nitrogen impacts on vegetation–critical evaluation and recommendations *Sci. Total Environ.* **603** 785–92

Büker P *et al* 2015 New flux based dose–response relationships for ozone for European forest tree species *Environ. Pollut.* **206** 163–74

C3S-ERA5 2017 Fifth generation of ECMWF atmospheric reanalyses of the global climate *Copernicus Climate Change Service Climate Data Store (CDS)* (available at: https://cds.climate.copernicus.eu/cdsapp#!/home)

Calori G, Clemente M, De Maria R, Finardi S, Lollobrigida F and Tinarelli G 2006 Air quality integrated modeling in Turin urban area *Environ. Model. Softw.* **21** 468–76

Chatani S *et al* 2014 Photochemical roles of rapid economic growth and potential abatement strategies on tropospheric ozone over south and east Asia in 2030 *Atmos. Chem. Phys.* **14** 9259–77

CLRTAP 2017 Mapping critical levels for vegetation, chapter III of manual on methodologies and criteria for modelling and mapping critical loads and levels and air pollution effects, risks and trends *UNECE Convention on Long-range Transboundary Air Pollution* (available at: http://icpvegetation.ceh.ac.uk/)

Cohen A J *et al* 2017 Estimates and 25–year trends of the global burden of disease attributable to ambient air pollution: an analysis of data from the global burden of diseases study 2015 *Lancet* **389** 1907–18

Colette A *et al* 2011 Air quality trends in Europe over the past decade: a first multi-model assessment *Atmos. Chem. Phys.* **11** 11657–78

Cooper O R, Gao R S, Tarasick D, Leblanc T and Sweeney C 2012 Long-term ozone trends at rural ozone monitoring sites across the United States, 1990–2010 *J. Geophys. Res.: Atmos.* **117** D22307

De Marco A, Sicard P, Fares S, Tuovinen J P, Anav A and Paoletti E 2016 Assessing the role of soil water limitation in determining the phytotoxic ozone dose (PODY) thresholds *Atmos. Environ.* **147** 88–97

De Marco A, Sicard P, Vitale M, Carriero G, Renou C and Paoletti E 2015 Metrics of ozone risk assessment for Southern European forests: canopy moisture content as a potential plant response indicator *Atmos. Environ.* **120** 182–90

Ding Y and Chan J 2005 The East Asian summer monsoon: an overview *Meteorol. Atmos. Phys.* **89** 117–42

Duncan B N, Lamsal L N, Thompson A M, Yoshida Y, Lu Z, Streets D G and Pickering K E 2016 A space-based, high-resolution view of notable changes in urban NOx pollution around the world (2005–2014) *J. Geophys. Res.: Atmos.* **121** 976–96

Emberson L D, Buker P and Ashmore M R 2007 Assessing the risk caused by ground level ozone to European forest trees: a case study in pine, beech and oak across different climate regions *Environ. Pollut.* **147** 454–66

Emmons L K *et al* 2010 Description and evaluation of the model for ozone and related chemical tracers, version 4 (MOZART-4) *Geosci. Model Dev.* **3** 43–67

Engardt M 2008 Modelling of near-surface ozone over South Asia *J. Atmos. Chem.* **59** 61–80

EPA 2007 Review of the national ambient air quality standards for ozone: policy assessment of scientific and technical information OAQPS Staff Paper U.S. Environmental Protection Agency, Office of Air Quality Planning and Standards, Research Triangle Park, North Carolina Publication No. EPA-452/R-07-003 p 603

Fang J Y, Chen A P, Peng C H, Zhao S Q and Ci L J 2001 Changes in forest biomass carbon storage in China between 1949 and 1998 *Science* **292** 2320–2

Feng Z, De Marco A, Anav A, Gualtieri M, Sicard P, Tian H, Fornasier F, Tao F, Guo A and Paoletti E 2019 Economic losses due to ozone impacts on human health, forest productivity and crop yield across China *Environ. Int.* **131** 9

Feng Z, Paoletti E, Bytnerowicz A and Harmens H 2015 Editorial Ozone and plants *Environ. Pollut.* **202** 215–6

Fu Y and Tai A P K 2015 Impact of climate and land cover changes on tropospheric ozone air quality and public health in East Asia between 1980 and 2010 *Atmos. Chem. Phys.* **15** 10093–106

Gaudel A *et al* 2018 Tropospheric ozone assessment report: present-day distribution and trends of tropospheric ozone relevant to climate and global atmospheric chemistry model evaluation *Elementa* **6** 59

Grell G A, Peckham S E, Schmitz R, Mckeen S A, Frost G, Skamarock W C and Eder B 2005 Fully coupled 'online' chemistry within the WRF model *Atmos. Environ.* **39** 6957–75

Guenther A B, Jiang X, Heald C L, Sakulyanontvittaya T, Duhl T, Emmons L K and Wang X 2012 The model of emissions of gases and aerosols from nature version 2.1 (MEGAN2.1): an extended and updated framework for modeling biogenic emissions *Geosci. Model Dev.* **5** 1471–92

Haase D *et al* 2014 A quantitative review of urban ecosystem service assessments: concepts, models, and implementation *Ambio* **43** 413–33

Han Z 2007 A regional air quality model: evaluation and simulation of O3 and relevant gaseous species in East Asia during spring 2001 *Environ. Model. Softw.* **22** 1328–36

Hoesly R M *et al* 2018 Historical (1750–2014) anthropogenic emissions of reactive gases and aerosols from the community emissions data system (CEDS) *Geosci. Model Dev.* **11** 369–408

Hoshika Y, Fares S, Savi F, Gruening C, Goded I, De Marco A, Sicard P and Paoletti E 2017 Stomatal conductance models for ozone risk assessment at canopy level in two Mediterranean evergreen forests *Agric. For. Meteorol.* **234–5** 212–21

Hoshika Y, Shimizu Y and Omasa K 2011 A comparison between stomatal ozone uptake and AOT40 of deciduous trees in Japan *iForest—Biogeosci. For.* **4** 128–35

Hu E Z, Gao F, Xin Y, Jia H X, Li K H, Hu J J and Feng Z 2015 Concentration- and flux-based ozone dose-response relationships for five poplar clones grown in North China *Environ. Pollut.* **207** 21–30

Hu J, Chen J, Ying Q and Zhang H 2016 One-year simulation of ozone and particulate matter in China using WRF/CMAQ modeling system *Atmos. Chem. Phys.* **16** 10333–50

Janssens-Maenhout G *et al* 2015 HTAP_v2.2: a mosaic of regional and global emission grid maps for 2008 and 2010 to study hemispheric transport of air pollution *Atmos. Chem. Phys.* **15** 11411–32

Kier G, Kreft H, Lee T M, Jetz W, Ibisch P L, Nowicki C, Mutke J and Barthlott W 2009 A global assessment of endemism and species richness across island and mainland regions *Proc. Natl Acad. Sci. USA* **106** 9322–7

Koike T, Watanabe M, Hoshika Y, Kitao M, Matsumura H, Funada R and Izuta T 2013 Chapter 17—effects of ozone on forest ecosystems in East and Southeast Asia *Dev. Environ. Sci.* **13** 371–90

Kottek M J, Grieser C, Beck R B and Rubel F 2006 World map of the Köppen-Geiger climate classification updated *Meteorol. Z.* **15** 259–63

Krotkov N A *et al* 2016 Aura OMI observations of regional SO2 and NO2 pollution changes from 2005 to 2015 *Atmos. Chem. Phys.* **16** 4605–29

Kumar R, Naja M, Pfister G G, Barth M C, Wiedinmyer C and Brasseur G P 2012 Simulations over south Asia using the weather research and forecasting model with chemistry (WRF-Chem): chemistry evaluation and initial results *Geosci. Model Dev.* **5** 619–48

Kunhikrishnan T, Lawrence M G, von Kuhlmann R, Wenig M O, Asman W A H, Richter A and Burrows J P 2006 Regional NOx emission strength for the Indian subcontinent and the impact of emissions from India and neighboring countries on regional O3 chemistry *J. Geophys. Res.: Atmos.* **111** D15301

Kurokawa J and Ohara T 2019 Long-term historical trends in air pollutant emissions in Asia: regional emission inventory in Asia (REAS) version 3.1 (available at: www.atmos-chem-phys-discuss.net›acp–2019–1122)

Lamarque J F *et al* 2013 The atmospheric chemistry and climate model intercomparison project (ACCMIP): overview and description of models, simulations and climate diagnostics *Geosci. Model Dev.* **6** 179–206

Lefohn A S *et al* 2018 Tropospheric ozone assessment report: global ozone metrics for climate change, human health, and crop/ecosystem research *Elementa* **6** 28

Lefohn A S, Shadwick D and Oltmans S J 2010 Characterizing changes in surface ozone levels in metropolitan and rural areas in the United States for 1980–2008 and 1994–2008 *Atmos. Environ.* **44** 5199–210

Li J, Wang Z, Akimoto H, Gao C, Pochanart P and Wang X 2007 Modeling study of ozone seasonal cycle in lower troposphere over east Asia *J. Geophys. Res.* **112** D22S25

Li K, Liao H, Mao Y H and Ridley D A 2016 Sectoral and regional contributions to black carbon and its direct radiative forcing in China *Atmos. Environ.* **124** 351–66

Li P, Feng Z, Catalayud V, Yuan X, Xu Y and Paoletti E 2017 A meta-analysis on growth, physiological, and biochemical responses of woody species to ground-level ozone highlights the role of plant functional types *Plant Cell Environ.* **40** 2369–80

Liao H and Shang J 2015 Regional warming by black carbon and tropospheric ozone: a review of progresses and research challenges in China *J. Meteorol. Res.* **29** 525–45

Lin M, Horowitz L, Payton R, Fiore A and Tonnesen G 2017 US surface ozone trends and extremes from 1980 to 2014: quantifying the roles of rising Asian emissions, domestic controls, wildfires, and climate *Atmos. Chem. Phys.* **17** 2943–70

Liu Y and Wang T 2020 Worsening urban ozone pollution in China from 2013 to 2017—part 2: the effects of emission changes and implications for multi-pollutant control *Atmos. Chem. Phys.* **20** 6323–37

Lu X, Hong J, Zhang L, Cooper O R, Schultz M G, Xu X, Wang T, Gao M, Zhao Y and Zhang Y 2018 Severe surface ozone pollution in China: a global perspective *Environ. Sci. Technol. Lett.* **5** 487–94

Melillo J, Mcguire A, Kicklighter D, Moore B, Vorosmarty C J and Schloss A L 1993 Global climate change and terrestrial net primary production *Nature* **363** 234–40

Mills G *et al* 2018 Tropospheric ozone assessment report: present-day tropospheric ozone distribution and trends relevant to vegetation *Elementa* **6** 47

Miranda A, Silveira C, Ferreira J, Monteiro A, Lopes D, Relvas H, Borrego C and Roebeling P 2015 Current air quality plans in Europe designed to support air quality management policies *Atmos. Pollut. Res.* **6** 434–43

Myers N, Mittermeier R A, Mittermeier C G, da Fonseca G A B and Kent J 2000 Biodiversity hotspots for conservation priorities *Nature* **403** 853–8

Nemani R R, Keeling C D, Hashimoto H, Jolly W M, Piper S C, Tucker C J and Myneni R B 2003 Running climate-driven increases in global terrestrial net primary production from 1982 to 1999 *Science* **300** 1560–3

Oksanen E, Pandey V, Pandey A K, Keski-Saari S, Kontunen-Soppel S and Sharma C 2013 Impacts of increasing ozone on Indian plants *Environ. Pollut.* **177** 189–200

Paoletti E *et al* 2019 Toward stomatal–flux based forest protection against ozone: the MOTTLES approach *Sci. Total Environ.* **691** 516–27

Paoletti E, De Marco A, Beddows D C S, Harrison R M and Manning W J 2014 Ozone levels in European and USA cities are increasing more than at rural sites, while peak values are decreasing *Environ. Pollut.* **192** 295–9

Paoletti E and Manning W J 2007 Toward a biologically significant and usable standard for ozone that will also protect plants *Environ. Pollut.* **150** 85–95

Park R J, Hong S K, Kwon H A, Kim S, Guenther A, Woo J H and Loughner C P 2014 An evaluation of ozone dry deposition simulations in East Asia *Atmos. Chem. Phys.* **14** 7929–40

Park R J and Kim S-W 2014 Air quality modeling in East Asia: present issues and future directions *Asia-Pac. J. Atmos. Sci.* **50** 105–20

Qiao X, Guo H, Wang P, Tang Y, Ying Q, Zhao X, Deng W and Zhang H 2019 Fine particulate matter and ozone pollution in the 18 cities of the Sichuan Basin in Southwestern China: model performance and characteristics *Aerosol Air Qual. Res.* **19** 2308–19

Reis S, Nitter S and Friedrich R 2005 Innovative approaches in integrated assessment modelling of European air pollution

control strategies—implications of dealing with multi-pollutant multi-effect problems *Environ. Model. Softw.* **20** 1524–31
Screpanti A and De Marco A 2009 Corrosion on cultural heritage buildings in Italy: a role for ozone? *Environ. Pollut.* **157** 1513–20
Shang B, Feng Z, Li P, Yuan X, Xu Y and Calatayud V 2017 Ozone exposure- and flux-based response relationships with photosynthesis, leaf morphology and biomass in two poplar clones *Sci. Total Environ.* **603–4** 185–95
Sharma S, Chatani S, Mahtta R, Goel A and Kumar A 2016 Sensitivity analysis of ground level ozone in India using WRF-CMAQ models *Atmos. Environ.* **131** 29–40
Sheel V, Lal S, Richter A and Burrows J P 2010 Comparison of satellite observed tropospheric NO2 over India with model simulations *Atmos. Environ.* **44** 3314–21
Sicard P, Anav A, De Marco A and Paoletti E 2017 Projected global tropospheric ozone impacts on vegetation under different emission and climate scenarios *Atmos. Chem. Phys.* **17** 12177–96
Sicard P, Crippa P, De Marco A, Castruccio S, Giani P, Cuesta J, Paoletti E, Feng Z and Anav A 2020 High spatial resolution WRF-Chem model over Asia: physics and chemistry evaluation *Atmos. Environ.* accepted
Sicard P, De Marco A, Dalstein-Richier L, Tagliaferro F, Renou C and Paoletti E 2016 An epidemiological assessment of stomatal ozone flux-based critical levels for visible ozone injury in Southern European forests *Sci. Total Environ.* **541** 729–41
Sicard P, De Marco A, Troussier F, Renou C, Vas N and Paoletti E 2013 Decrease in surface ozone concentrations at Mediterranean remote sites and increase in the cities *Atmos. Environ.* **79** 705–15
Simpson D, Ashmore M R, Emberson L and Tuovinen J P 2007 A comparison of two different approaches for mapping potential ozone damage to vegetation. A model study *Environ. Pollut.* **146** 715–25
Skamarock W C and Klemp J B 2008 A time-split nonhydrostatic atmospheric model for weather research and forecasting applications *J. Comput. Phys.* **227** 3465–85
Surendran D E, Ghude S D, Beig G, Emmons L K, Jena C, Kumar R, Pfister G G and Chate D M 2015 Air quality simulation over South Asia using hemispheric transport of air pollution version-2 (HTAP-v2) emission inventory and model for ozone and related chemical tracers (MOZART-4) *Atmos. Environ.* **122** 357–72
Tang H, Takigawa M, Liu G, Zhu J and Kobayashi K 2013 A projection of ozone-induced wheat production loss in China and India for the years 2000 and 2020 with exposure-based and flux-based approaches *Glob. Change Biol.* **19** 2739–52
Tai A P K, Val Martin M and Heald C L 2014 Threat to future global food security from climate change and ozone air pollution *Nat. Clim. Change* **4** 817–21
Tuovinen J-P, Simpson D, Emberson L, Ashmore M and Gerosa G 2007 Robustness of modelled ozone exposures and doses *Environ. Pollut.* **146** 578–86
US Federal Register 2015 National ambient air quality standards for ozone, 40 CFR part 50, 51, 52, 53, and 58 pp 65292–468
Wang Y, Konopka P, Liu Y, Chen H, Müller R, Plöger F, Riese M, Cai Z and Lü D 2012 Tropospheric ozone trend over Beijing from 2002–2010: ozonesonde measurements and modeling analysis *Atmos. Chem. Phys.* **12** 8389–99
Wiedinmyer C, Akagi S K, Yokelson R J, Emmons L K, Al-Saadi J A, Orlando J J and Soja A J 2011 The fire inventory from NCAR (FINN): a high resolution global model to estimate the emissions from open burning *Geosci. Model Dev.* **4** 625–41
World Health Organisation 2013 Review of evidence on health aspects of air pollution—REVIHAAP project *Technical Report* (Copenhagen, Denmark: World Health Organization, Regional Office for Europe)
Xu B, Guo Z, Piao S and Fang J 2010 Biomass carbon stocks in China's forests between 2000 and 2050: a prediction based on forest biomass–age relationships *Sci. China Life Sci.* **53** 776–83
Yan Y, Pozzer A, Ojha N, Lin J and Lelieveld J 2019 Trend reversal from high-to-low and from rural-to-urban ozone concentrations over Europe *Atmos. Environ.* **213** 25–36
Yu G, Chen Z, Piao S, Peng C, Ciais P, Wang Q, Li X and Zhu X 2014 High carbon dioxide uptake by subtropical forest ecosystems in the East Asian monsoon region *Proc. Natl Acad. Sci.* **111** 4910–5
Zeng Y, Cao Y, Qiao X, Seyler B C and Tang Y 2019 Air pollution reduction in China: recent success but great challenge for the future *Sci. Total Environ.* **663** 329–37
Zhang K, Song C, Zhang Y and Zhang Q 2017 Natural disasters and economic development drive forest dynamics and transition in China *For. Policy Econ.* **76** 56–64
Zhu Z, Bi J, Pan Y, Ganguly S, Anav A, Xu L, Samanta A, Piao S, Nemani R R and Myneni R B 2013 Global data sets of vegetation leaf area index (LAI)3g and fraction of photosynthetically active radiation (FPAR)3g derived from global inventory modeling and mapping studies (GIMMS) normalized difference vegetation index (NDVI3g) for the period 1981 to 2011 *Remote Sens.* **5** 927–48